Journal of Molecular Structure 1262 (2022) 133084

Contents lists available at ScienceDirect

Journal of Molecular Structure

journal homepage: www.elsevier.com/locate/molstr

Quantum computational, spectroscopic investigation, molecular docking, and *in vitro* pharmacological studies of sulfonamide Schiff base

Subrata Paul[a], Md. Ashraful Alam[a], Tarun Kumar Pal[a,*], Md. Najem Uddin[b], Md. Monirul Islam[a], Md. Chanmiya Sheikh[c]

[a] Department of Chemistry, Rajshahi University of Engineering & Technology, Bangladesh
[b] Pharmaceutical Sciences Research Division, BCSIR laboratories (Dhaka), Bangladesh Council of Scientific and Industrial Research (BCSIR), Bangladesh
[c] Department of Chemistry, University of Rajshahi, Bangladesh

ARTICLE INFO

Article history:
Received 19 January 2022
Revised 22 March 2022
Accepted 12 April 2022
Available online 16 April 2022

Keywords:
DFT
Single crystal X-ray
Cytotoxic activity
Pharmacophore sites
Antioxidant

ABSTRACT

A new Schiff base, (*E*)-4-((3,5-dibromo-2-hydroxybenzylidene)amino)-*N*-(5-methylisoxazol-3-yl)benzenesulfonamide was synthesized and characterized by various physico-chemical, X-ray crystallography and DFT methods. The experimental findings were compared with the computed data. The characteristic azomethine band was found at 1616 cm^{-1} in the experimental FTIR spectrum. The double bond distance between C7=N1 was 1.277(5) Å. Single X-ray crystallography data indicated that the crystal system of the compound was monoclinic with space group $P2_1/c$. The experimental values were well correlated with the computed ones. The kinetic stability of the compound was high due to the larger HOMO-LUMO energy gap. Molecular docking and POM (Petra/Osiris/Molinspiration) investigation of the compound were also performed. POM analysis identified one antibacterial and two antitumor pharmacophore sites in the compound. It exhibited higher binding energy than the reference drug in molecular docking study. The compound followed Lipinski's rule of five and exhibited promising drug-like character and drug score. Moreover, *in vitro* anticancer, antibacterial, antifungal, anti-inflammatory and antioxidant properties of the compound were also carried out. It showed good antibacterial effects against *S. aureus* and *S. typhi* strains. In case of antifungal activity, the compound showed moderate inhibitory activity against both *A. niger* and *A. flavus* strains. Besides, it has the capability to stabilize the human red blood cell membrane in hypotonic solution and protect hemolysis. The highest cytotoxic activity of the compound with IC_{50} value of 65.344 μg/mL was observed against A549 lung cancer cells. Finally, the compound showed moderate antioxidant activity with IC_{50} value of 4.25 μM.

1. Introduction

Sulfonamide compounds contain sulfur in sulfonamide moiety directly attached to a benzene ring. Sulfamethoxazole is a well-known sulfonamide bacteriostatic antibiotic. It obstructs the formation of dihydrofolic acid from bacteria and is mainly used to treat urinary tract and gastrointestinal infections [1,2]. Recently, synthesis and characterization of large numbers of sulfamethoxazole derivatives have been remarkably emphasized to treat different bacterial diseases [2,3]. The condensation of sulfonamide compound with at least one amino group and active carbonyl compound can produce biologically active sulfonamide Schiff base substance. The presence of azomethine (–CH=N–) and sulfonamide ($–SO_2NH–$) functional groups are believed to be responsible for their biological activity [4,5]. These compounds are used in pharmacological fields for various potential applications. Some sulfonamide compounds have been shown to have good antimicrobial activity against few pathogenic microorganisms [4–6]. In fact, Schiff base compounds, such as nifuroxazide and thiacetazone, are used in the treatment of tuberculosis [7]. These compounds are also utilized in the development of coordination chemistry. They also have the ability to form stable chelates with transition metal ions [3]. The resulting transition metal complexes with such ligands have gained considerable importance in material science, and bioinorganic chemistry [4,7]. Sulfonamide compounds are extensively used as antibacterial, antifungal, anticancer, anti-inflammatory and antiviral agents as well as HIV protease inhibitors [4,8–10]. Some sulfonamide derivatives are also well recognized as an antimetabolite. These compounds have also exhib-

* Corresponding author.
E-mail address: tkpchem@gmail.com (T.K. Pal).

https://doi.org/10.1016/j.molstruc.2022.133084
0022-2860/

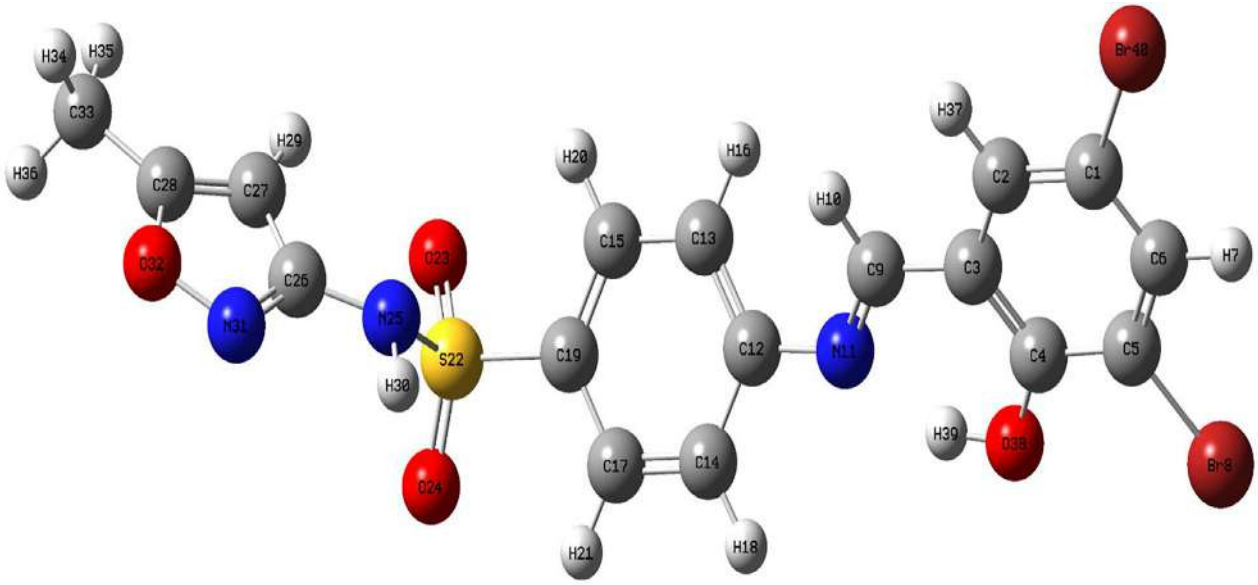

Fig. 1. Optimized geometry of the compound.

ited good cytotoxic effects against breast cancer cells [11]. Several urinary tract infections and gastrointestinal infections are clinically treated with sulfonamide compounds. Besides, some sulfonamide derivatives have shown good antioxidant activity [12]. Nowadays, scientists are greatly attracted to computational approaches to support the experimental shreds of evidence of chemical analysis. Therefore, the computational techniques are immensely utilized for the determination of the proposed geometry of the recently synthesized compounds. To the best of our knowledge, quantum computational calculation, comparison with experimental data, Hirshfeld surface, molecular docking, and *in vitro* pharmacological investigations of the compound have not been reported previously. In view of these facts, we have synthesized, characterized and reported the compound (Fig. 1) here in detail. Molecular docking studies and Petra/Osiris/Molinspiration (POM) analysis of the compound were also conducted. Drug-like character was evaluated by Lipinski's rule of five. Besides, the compound was tested against some pathogenic bacterial and fungal strains. Finally, *in vitro* anticancer, anti-inflammatory and antioxidant activities of the compound were also carried out.

2. Experimental procedure

2.1. Materials and methods

3,5-dibromosalicylaldehyde and sulfamethoxazole were purchased from Sigma-Aldrich. All chemicals and solvents were used without further purification. An open capillary method was used for the measuring of melting point of the compound. Fourier transform infrared (FTIR) spectroscopy was performed using a SHIMADZU IR Affinity-1S. The electronic spectrum was recorded in dichloromethane using PG Instruments CT60. The XRD pattern was taken by powder X-ray diffraction (D8 Advanced Bruker, Germany) with filtered Cu-Kα radiation (λ=1.5418 Å). The diffraction pattern was taken with a scanning step of 0.02°/s from 20 to 60° ^{1}H NMR (400 MHz) and ^{13}C NMR (100 MHz) spectra were scanned in dimethylsulfoxide on a JEOL JNM-ECZ400S and mass spectra were taken on a JEOL-JMS-D300 spectrometer, Okayama University of Science, Japan. disk diffusion method was used to evaluate antibacterial and antifungal activity of the compound. Cytotoxic activity was determined using trypan blue exclusion method and antioxidant activity was determined using 2,2-diphenyl-1-picrylhydrazyl (DPPH) method.

2.2. Synthesis and crystal growth

1 mmol 3,5-dibromosalicylaldehyde ethanolic solution was added to the ethanolic solution of sulfamethoxazole (1 mmol) with constant stirring (Scheme 1). The resulting solution was refluxed at 90°C for three hours. An orange color product was precipitated. Then it was filtered and washed with diethyl ether and dried under vacuum over anhydrous $CaCl_2$ to give (*E*)−4-((3,5-dibromo-2-hydroxybenzylidene)amino)-*N*-(thiazol-2-yl)benzenesulfonamide. Orange colored single crystals were found

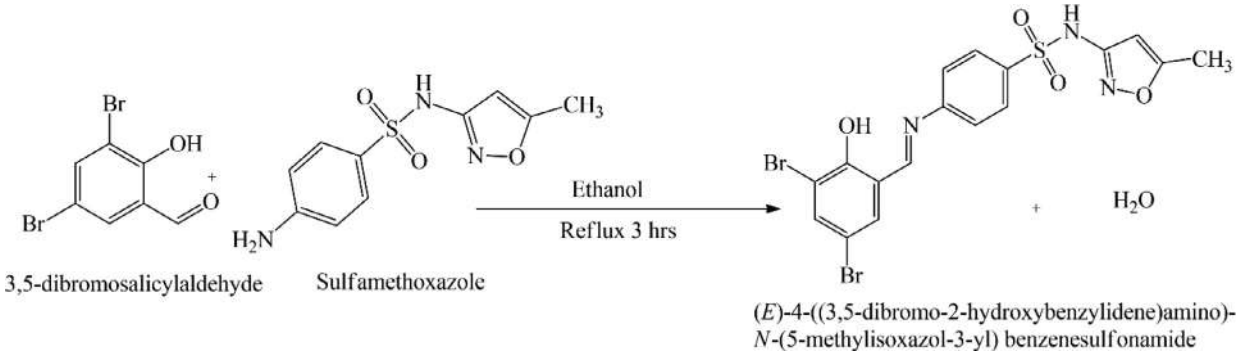

Scheme 1. Synthesis of the compound.

from dichloromethane and acetonitrile mixture in the ratio of 1:10 (*v:v*) by slow evaporation.

2.3. Crystal structure determination

A Rigaku R-AXIS RAPID diffractometer with Cu-Kα radiation of wavelength λ=1.54187 Å was used to collect X-ray diffraction data of the compound at 173 K. The direct methods were used to solve the crystal structure. The full-matrix least-squares method based on F^2 was used to refine the crystal structure. All the hydrogen atoms were positioned geometrically and refined isotropically using a riding model.

2.4. Computational methodology

The molecular structure of the compound (Fig. 1) was illustrated using GaussView 6.0.16 software [13]. GaussView 6.0.16 and Gaussian 09 W software [14] packages were applied for the quantum chemical calculations using DFT technique at B3LYP/6–31G+(d,p) basis set [15]. The frontier molecular orbitals, *i.e.,* highest occupied molecular orbital (HOMO) and lowest unoccupied molecular orbital (LUMO) energies as well as molecular electrostatic potential (MEP) were generated using GaussView software [13]. For the calculation of the electronic excitations TD-DFT method was applied. The vibrational frequencies were scaled by 0.9614 [16].

3. Results and discussion

The yield of the compound was 81.2% and melting point was 238°C. The compound was highly soluble in dichloromethane, chloroform, N,N-dimethylformamide (DMF), dimethylsulfoxide (DMSO) and moderately soluble in methanol, ethanol, and water.

3.1. FTIR spectra

The band attributed to the phenolic hydroxyl group of the compound was found at 3444 cm^{-1} in the experimental [17,18] and at 3539 cm^{-1} in the theoretical spectra (Fig. 2). The peak corresponds to azomethine group was observed at 1616 cm^{-1} [8,9,19], which is theoretically assigned at 1674 cm^{-1}. The asymmetric and symmetric bands of S—O bonds were found at 1340 and 1161 cm^{-1}, respectively [19–21] and the corresponding bands were found theoretically at 1367 and 1285 cm^{-1}. The computational results showed slightly at higher frequencies than the experimental ones for the respective groups, because the computational calculations were conducted at gas phase whereas experimental calculations were done in solid phase.

3.2. UV–vis studies

The UV–vis spectrum of the compound was carried out in the range of 200–800 nm. The two peaks observed at 220 and 245 nm [8,20] were assigned to $\pi-\pi^*$ electronic transition (Fig. 3). In contrast, theoretically a band was found at 330 nm. Experimentally another one band was observed at 270 nm, which may be attributed to $n-\pi^*$ electronic transitions [9,21]. Theoretically it was not found.

3.3. Crystal structure interpretation

The crystallographic data revealed that C7=N1 bond distance was 1.277(5) Å, which confirms its significant double bond character. The C8—N1 bond distance was 1.419(5) Å, which revealed the significant delocalization of the π-electron density on the azomethine portion of the compound. The obtained bond distance was almost the same with the computed value (1.282 Å) and the reported carbon-nitrogen double bond distance of similar compounds [18,22]. The compound existed in an *E*-configuration owing to the C = N double bond of azomethine group [23] (Fig. 4). In the compound, three aromatic units are present which are linked through sulfonamide (—NH—SO_2—) and azomethine (—HC=N—) groups. Phenolato unit is connected to aryl sulfonamide by the sulfonamide group and the oxazolyl unit is associated by the azomethine group. Two benzene rings of the compound made dihedral angle of 18.66° due to the double bond of C7=N1. The proton, H1 atom located on O1 formed a characteristic intramolecular hydrogen bond (O1—H1···N1) with graph-set notation S(6) [24]. Thus,

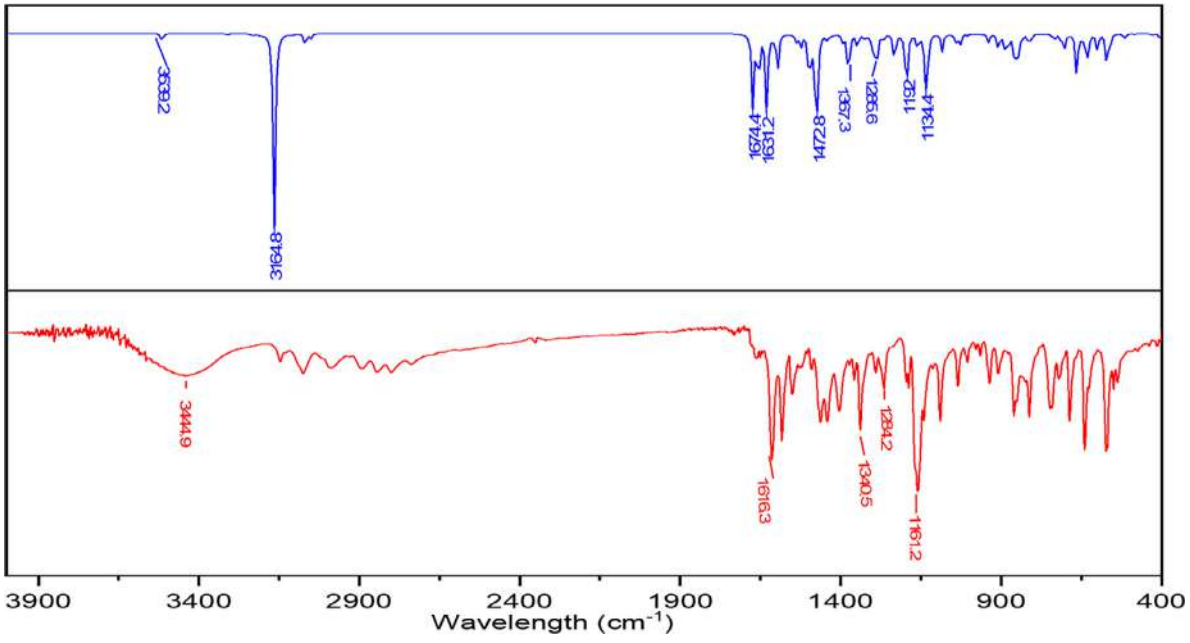

Fig. 2. Infrared spectrum of theoretical (top) and experimental (bottom) of the compound.

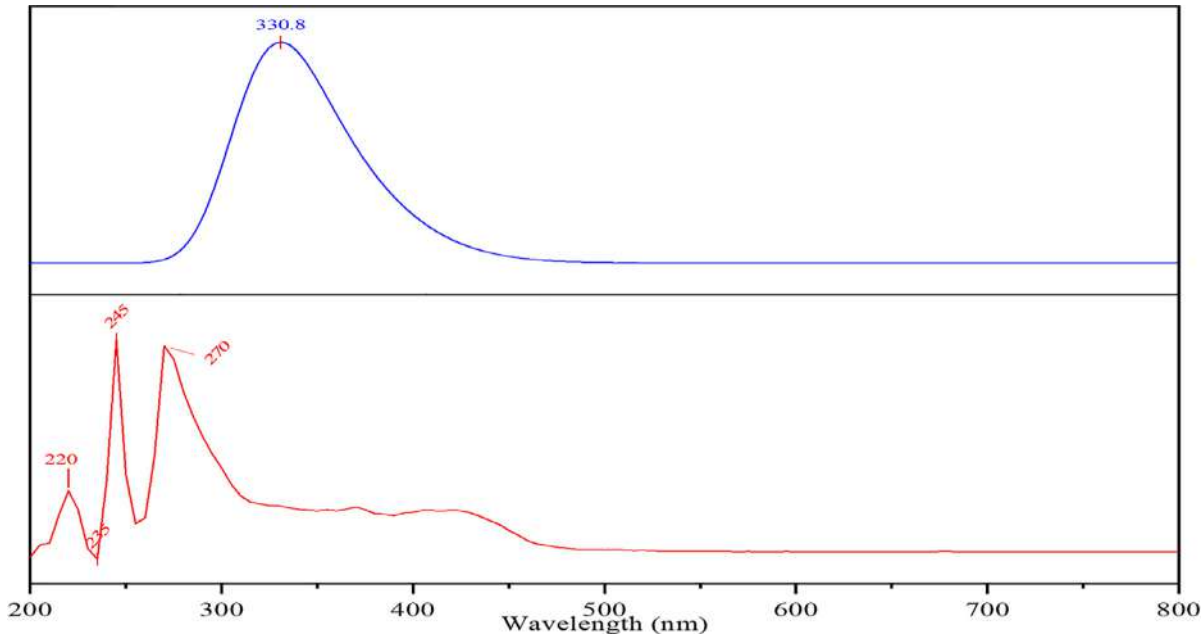

Fig. 3. UV–vis spectrum of the compound for theoretical (top) and experimental (bottom).

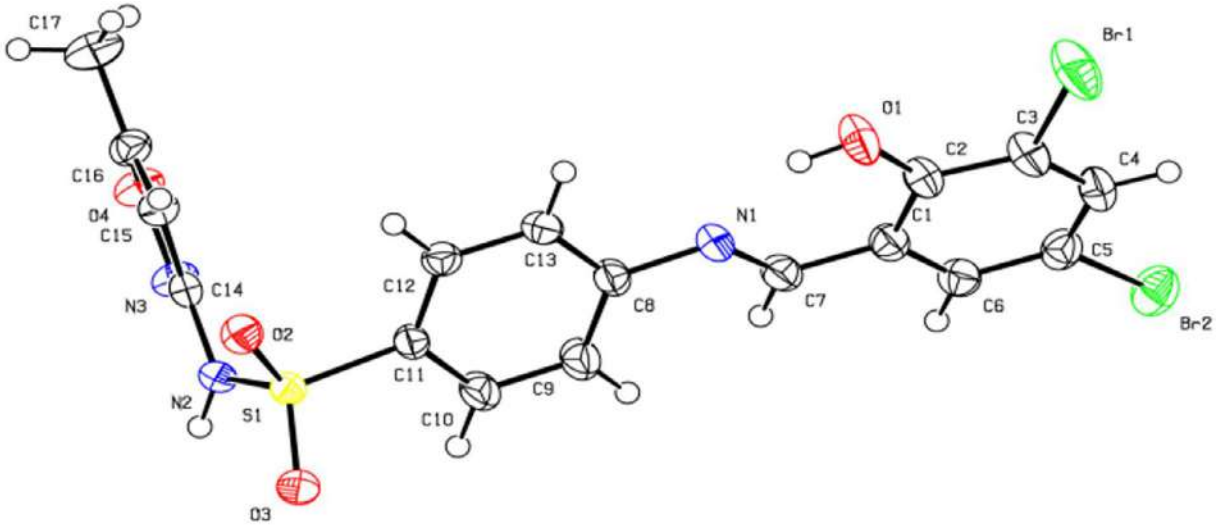

Fig. 4. ORTEP view of the compound.

two benzene rings and azomethine group were effectively coplanar. Moreover, the configuration around the S1 atom of the sulfonamide unit deviates from ideal tetrahedron geometry. Thus, the largest deviation is 120.33(15)° in the angle of O2-S1-O3 due to the repulsion of negatively charged oxygen atoms. The torsion angles C6—C1—C7—N1 and N1—C8—C9—C10 are 179.8 (3)° and 175.2 (3)°, respectively. The S1—C11 bond length was 1.759(3) Å, which was comparable to the reported normal single-bond value of similar compounds [24,25]. The compound was stabilized owing to the presence of intramolecular hydrogen bonds and weak $\pi-\pi$ stacking interactions between aromatic rings. In the crystal, inversion dimers with $R_2^2(8)$ ring motive were formed due to link of two molecules via pairs of N—H···N hydrogen bonds. From the correlation diagram, the linearity relation was found between the computed and experimental values. For the bond distance and bond angle, the correlation coefficient (R^2) values were found to be 0.9824 and 0.9254, respectively. Thus the experimental results were well consistent with the computed one.

3.4. NMR spectra

The azomethine proton signal was found at 8.94 ppm in ^{1}H NMR spectrum (Fig. 5). The compound exhibited a peak at 10.93 ppm owing to phenolic O—H proton. The peak at 10.02 ppm was found due to SO_2NH proton. The peaks were found to be in the range 6.51—6.55 and 7.93—8.04 ppm for bromo–phenyl and azomethine linkage-phenyl protons. Besides, methylisoxazole and isoxazole protons were observed at 2.28 and 6.12 ppm, respectively. In ^{13}C NMR, azomethine, methylisoxazole and C2 of bromo–phenyl carbon signals were found at 169.9, 12.0 and 157.9 ppm, respectively (Fig. 6). C3, C4 and C5 of isoxazole carbons showed their signals at 128.3, 95.3 and 193.2 ppm. Both C4 and C6 carbons of bromo–phenyl were exhibited a sharp signal at 133.1 ppm. Moreover, C2 and C6 as well as C3 and C5 of N-phenyl carbons showed intense signals at 112.6 and 128.8 ppm, respectively. Afterward, C1, C3 and C5 of bromo–phenyl carbon signals were found at 124.2, 124.5 and 122.5 ppm, respectively. C1 and C4 of N-phenyl

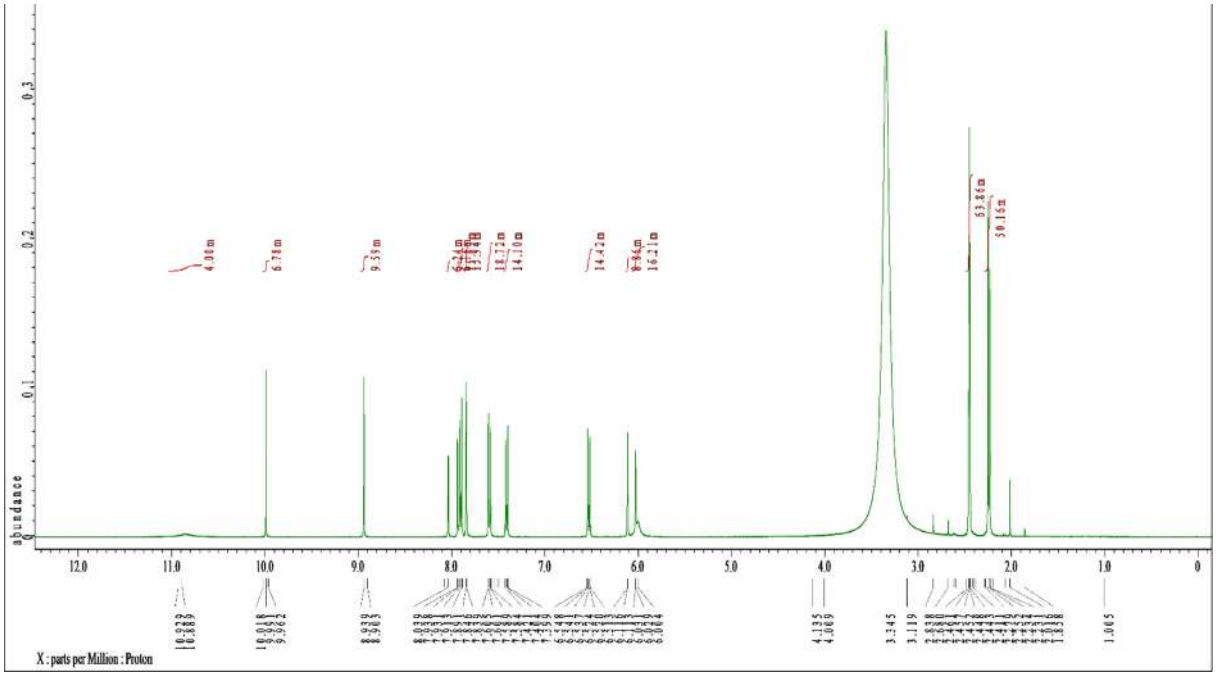

Fig. 5. ^{1}H NMR spectrum of the compound.

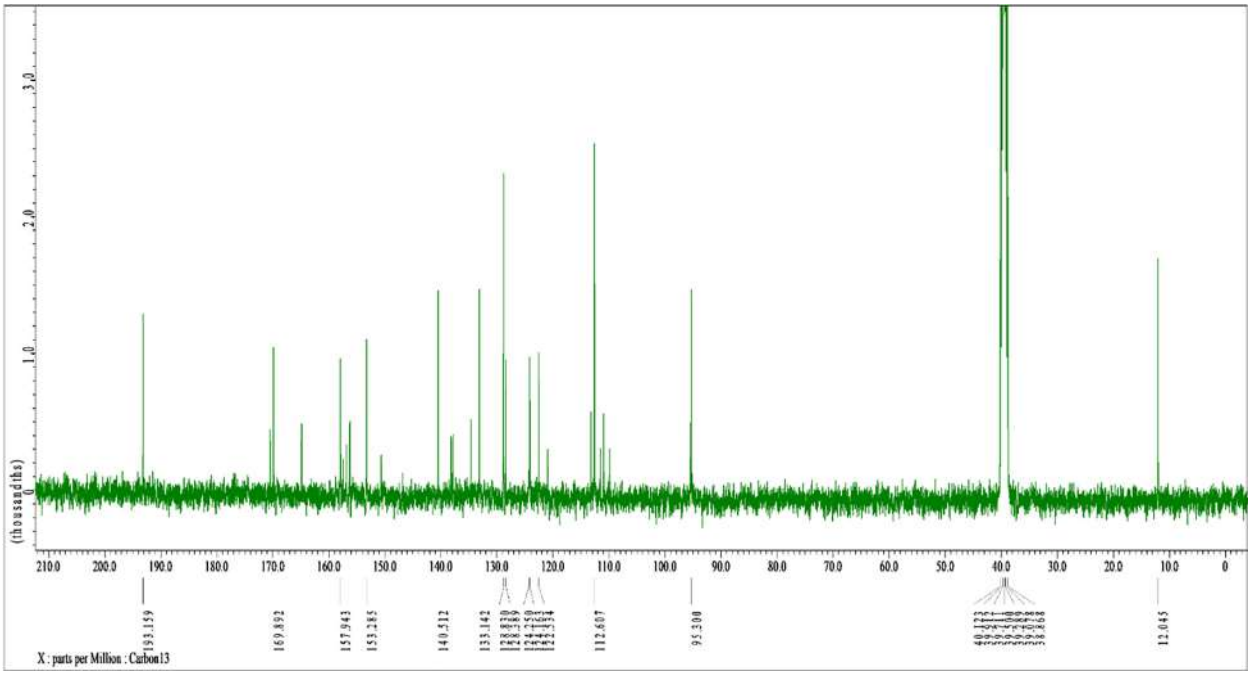

Fig. 6. ^{13}C NMR spectrum of the compound.

carbon showed their characteristics peaks at 153.3 and 140.5 ppm, respectively.

3.5. Mass spectra

The mass spectrum provides information about the compound such as fragmentation pattern, molecular mass as well as structure of a compound. The molecular ion peak of the compound was found at 515 amu and base peak was found at 394 amu (Fig. 7). The compound also displayed various peaks at 434, 194, 156 and 77 amu owing to its corresponding fragments. Therefore, molecular ion peak and other peaks were in compliance with the destined molecular formula.

3.6. Powder X-ray diffraction

The experimental powder X-ray diffraction (XRD) data was analyzed using PowderX program [26]. The average crystallite size of the compound was determined from most sharp peaks of diffractogram using Sherrer's equation [27]. The XRD findings indicated that all the diffraction peaks were quite well indexed to monoclinic structure with space group $P2_1/c$. The sharp peaks with high intensity indicated that the compound was crystalline in nature.

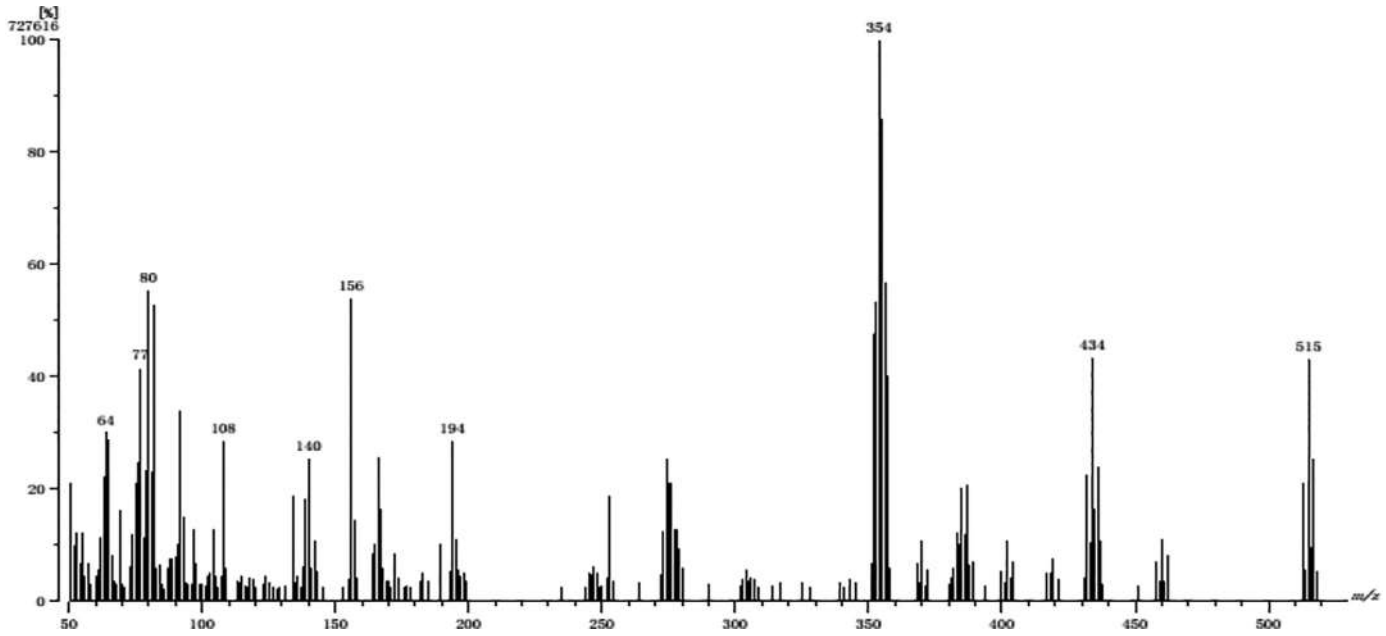

Fig. 7. Mass spectrum of the compound.

Crystalline size of the compound was 33.06 nm suggesting that it has nanocrystalline phase.

3.7. Frontier molecular orbitals and global reactivity descriptors

The highest filled molecular orbital energy (E_{HOMO}) and the lowest empty molecular orbital energy (E_{LUMO}), are known as frontier molecular orbitals (FMOs). The energy gap between LUMO and HOMO orbitals is an important parameter to explain the reactivity and stability of any chemical species. Generally, energy gap is related inversely to the reactivity and directly to the stability of any chemical species. Compounds having small gaps are chemically soft, unstable and more reactive and those with large gaps are chemically hard, stable and less reactive [19,28,29]. Therefore, the energy and energy gap of the compound were ascertained and the corresponding molecular orbital pictographic display was presented in Fig. 8. The results of the FMOs and various parameters were given in Table 1. The energies of HOMO and LUMO were −6.706 and −2.998 *eV*, respectively. Therefore, the energy gap of the compound was found to be 3.708 *eV*. The huge energy gap of the compound indicated that it was chemically more stable and less reactive. Besides, high chemical reactivity could be defined by applying greater values of chemical potential and electrophilicity index. Besides, chemical reactivity could be described by the chemical hardness, chemical potential and electrophilicity index. The more negative value of chemical potential revealed the higher stability of the compound. The electron giving and accepting ability of any chemical species can be defined by ionization potential and electron affinity respectively, which are related to HOMO and LUMO energies [28,30]. Ionization potential of the compound was numerically greater in magnitude than its electron affinity indicating its good electron donating ability. The findings of electrophilicity index support it.

Table 1
Global reactivity descriptors of the compound (in *eV*).

Parameters	Value
HOMO energy	−6.706
LUMO energy	−2.998
Energy gap ($\Delta E_{LUMO\text{-}HUMO}$)	3.708
Ionization potential (I)	6.706
Electron affinity (A)	2.998
Chemical hardness (η)	1.854
Chemical softness (S) (eV^{-1})	0.270
Chemical potential (μ)	−4.852
Electronegativity (χ)	4.852
Electrophilicity index (ω)	6.349

In the compound, HOMO orbitals were populated on a halogenated benzene ring, oxygen atom of hydroxyl group, azomethine group and slightly extended up to adjacent benzene ring (Fig. 8). Whereas, LUMO orbitals were colonized on the both benzene rings, azomethine group and oxygen atom of hydroxyl group.

3.8. Molecular electrostatic potential (MEP) surface

The molecular electrostatic potential method informs about the relative reactivity of various positions in a compound, at which nucleophilic and electrophilic species can attack [31,32]. The molecular electrostatic potential is a pictorial representation of the electronic density distribution over the investigated molecule. The electronic properties, dipole moment and molecular polarizability of a molecule are highly dependent on MEP [31,33]. In the compound, electron rich and electron poor regions were indicated by red and blue colors, respectively. The polarization effect was visible in the compound. In this case, the negative potential areas were situated over the oxygen, nitrogen and bromine atoms (Fig. 9). Whereas the positive potential areas were positioned over the hydrogen atoms. The nitrogen atom of the azomethine group showed less electronegative potential than the other atoms. However, the light green and sky-blue areas represent the neutral electrostatic region in the compound.

3.9. Harmonic oscillator model of aromaticity (HOMA) index

The aromaticity is the simplest, successful and popular term in organic chemistry. The aromaticity of the cyclic and planar organic compounds can be calculated with the help of a harmonic oscillator model of aromaticity [34]. HOMA index of the compound has been calculated as per the following relations:

$$\mathrm{HOMA} = 1 - \frac{1}{n}\sum_{i}^{n}\alpha\,(R_{opt} - R_i)^2 = 1 - \mathrm{EN} - \mathrm{GEO} \qquad (1)$$

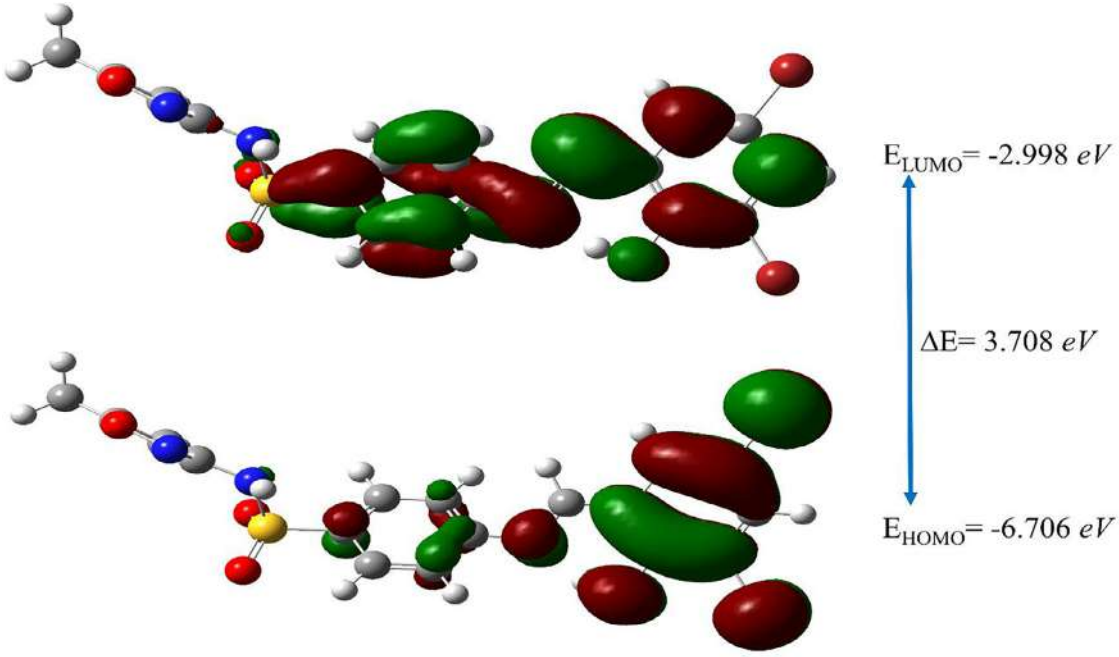

Fig. 8. HOMO and LUMO energy plot of the compound.

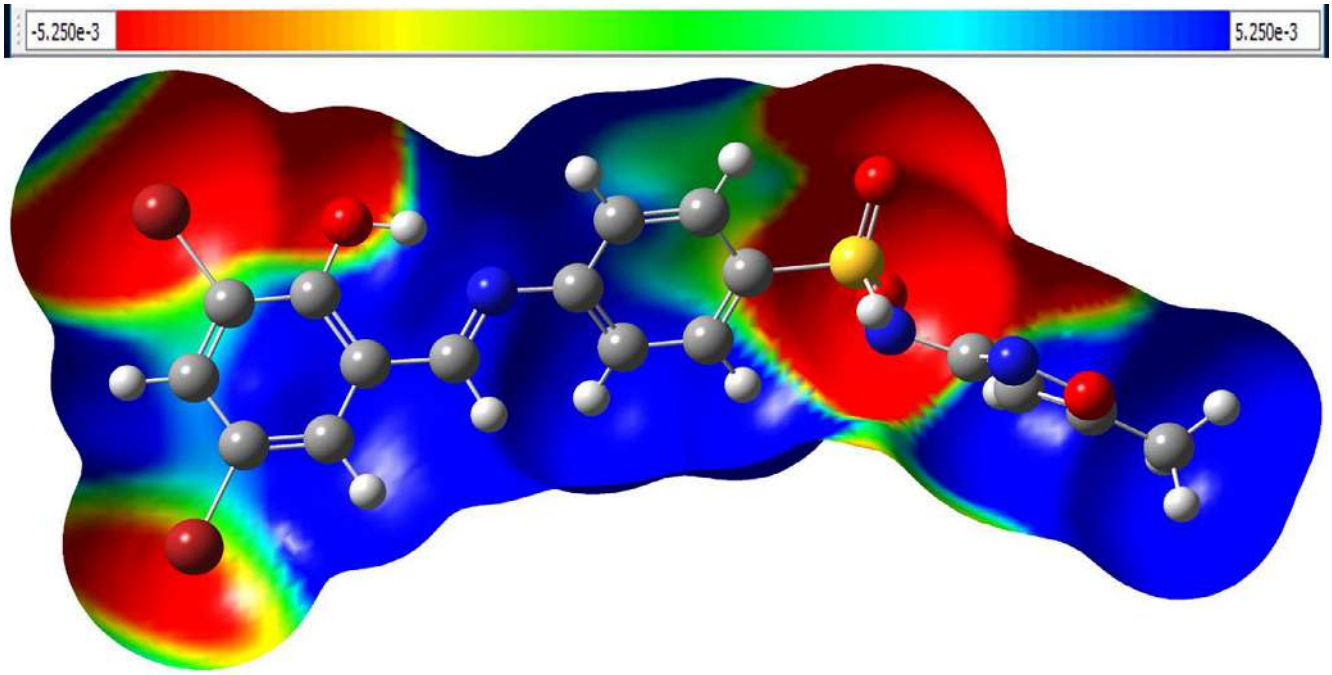

Fig. 9. MEP mapped of the compound.

Where

$$GEO = \frac{1}{n}\sum_{i}^{n}\alpha(R_{av} - R_i)^2 \quad (2)$$

and

$$EN = \alpha(R_{opt} - R_{av})^2 \quad (3)$$

The HOMA index value of an aromatic and non-aromatic compound should be close to unity and zero, respectively [34]. The experimental HOMA index value was 0.9316 for C1-C6 ring and 0.9952 for C12-C19 ring. Computationally it was found to be 0.9314 for C1-C6 ring and 0.9556 for C12-C19 ring. The C1-C6 ring showed slightly lower value of HOMA than the C12-C19 ring due to the existence of electron withdrawing substituent groups on the C1-C6 ring. Therefore, both rings are aromatic in nature and the compound exists in phenol-imine form.

3.10. Hirshfeld surface property

Hirshfeld surface analysis is widely used for the visualization of crystal structure and investigation of the intermolecular interac-

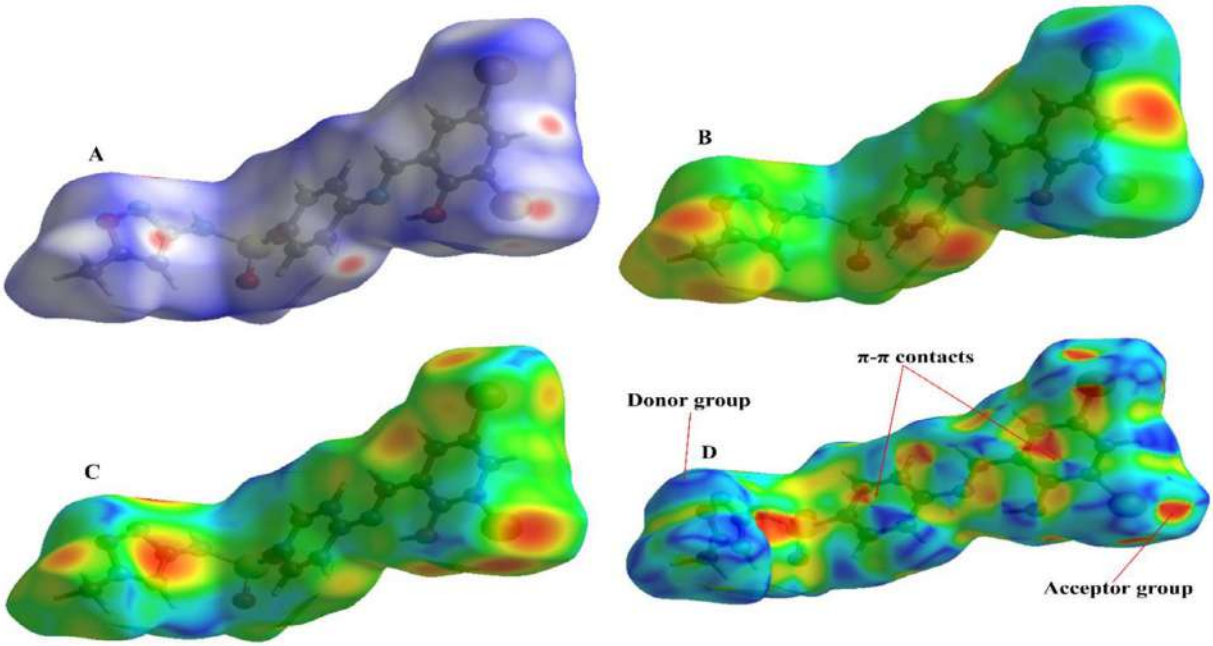

Fig. 10. View of Hirshfeld surface over (A) d_{norm}, (B) d_i, (C) d_e and (D) shape-index.

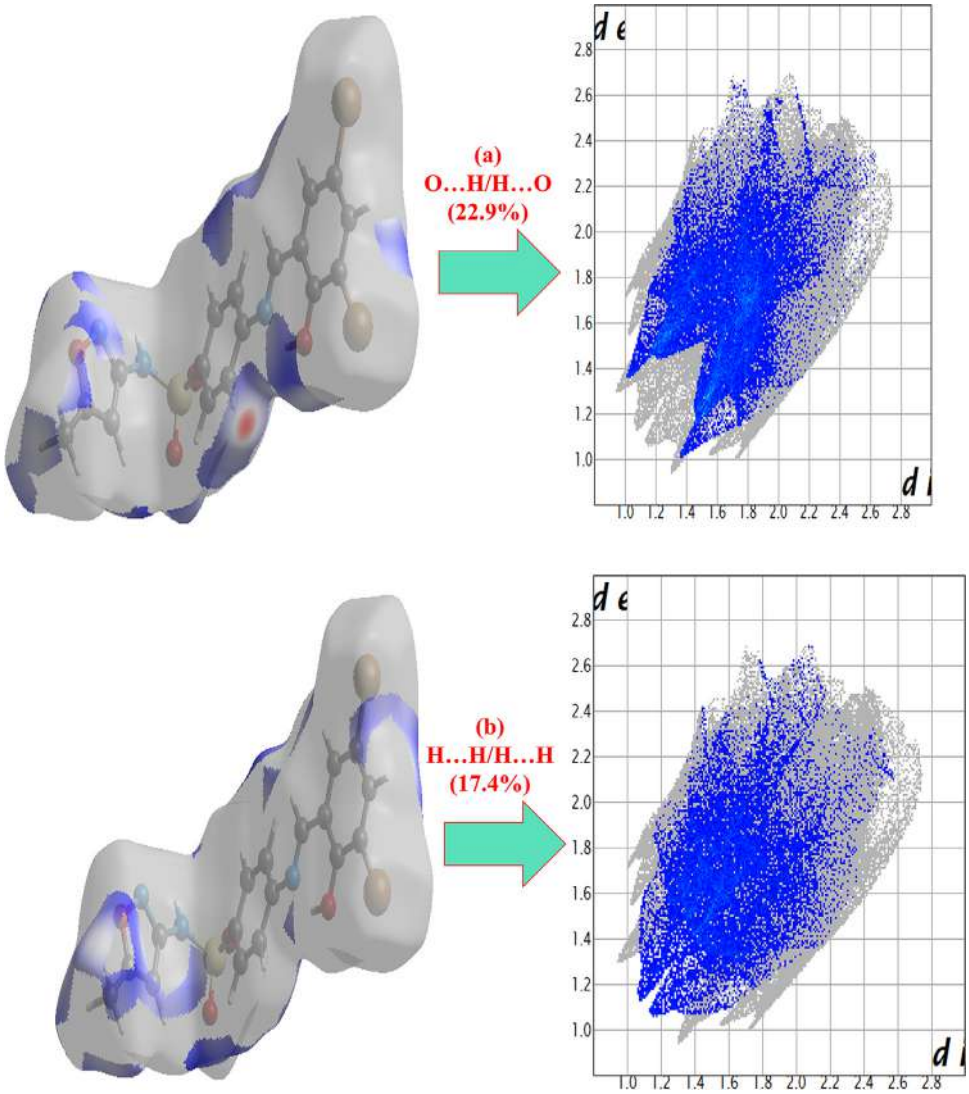

Fig. 11. Two-dimensional fingerprint plots with d_{norm} view of (a) O···H/H···O, (b) H···H/H···H, (c) C···H/H···C, and (d) N···H/H···N close contacts.

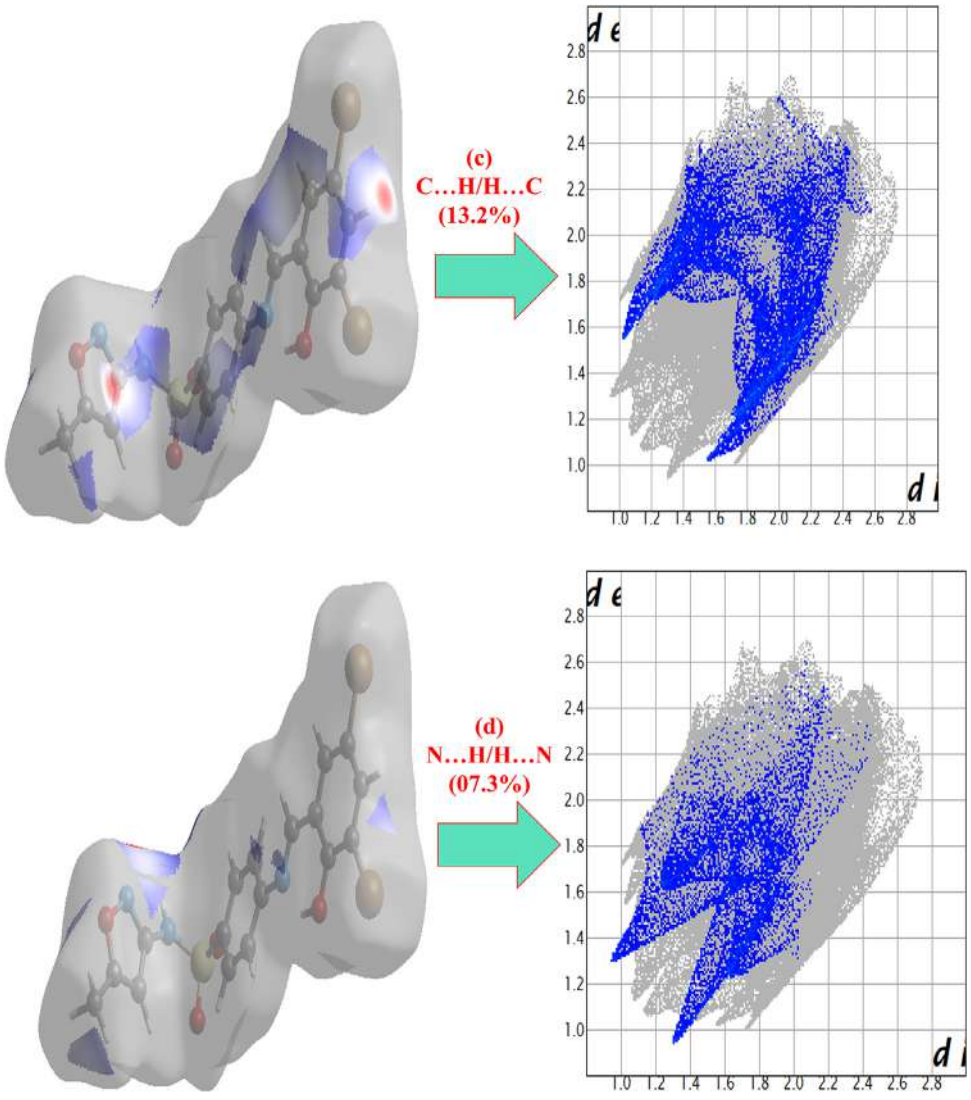

Fig. 11. Continued

tions in the crystalline material [35,36]. Crystal Explorer 17.5 software was used for the calculation of Hirshfeld surfaces and 2D fingerprint plots [37] which are depicted in Figs. 10 and 11, respectively. In the d_{norm} map, the characteristic intense red spots indicated that the intermolecular interactions are present in the compound. The hydrogen-donor and hydrogen-acceptor groups were indicated by the blue and red regions in the shape-index map, respectively (Fig. 10, D). Interactions between π-π are present in the compound, which is confirmed by the adjacent red and blue triangles. In case of 2D fingerprint plots map (Fig. 11), the O···H contacts create major contribution to the total Hirshfeld surface of the compound with 22.9%. Moreover, H···H, C···H and N···H contacts contributed 17.4, 13.2 and 7.3%, respectively towards the compound.

3.10. Molecular docking studies

Molecular docking simulation helps to develop new drug compound. It can also be expressed how a drug bind with the docking pocket of target protein. The molecular docking studies of the compound and reference drug (ciprofloxacin) were performed with pneumonia protein (4FQ4). The binding affinity of the compound and ciprofloxacin with 4FQ4 were −8.4 and −7.4 kcal/mol, respectively. The inhibition constants of the compound and ciprofloxacin were 0.70 and 1.89 μM, respectively. In the docking pocket, both ciprofloxacin and the applied compound formed two hydrogen bonds with the subjected protein via different amino acid residues. Ciprofloxacin interacted with Glu409 and Asn443 amino acid residues at distances 2.85 and 2.98 Å, respectively (Fig. 12). In addition, the reference drug showed hydrophobic interactions with Phe294, Asn299, Lys407, Phe298, Gln473, Lys297, Phe474 and Trp471 amino acids and on the other hand, the studied compound offered such interactions with Glu169, Arg310, Phe167, Glu165, Tyr307, Ser128 and Leu126 amino acids of the protein.

3.11. Petra/Osiris/Molinspiration (POM) analysis

In-silico pharmacokinetic study and prediction of drug-likeness save millions of dollars and time in drug design and development [38,39]. The drug molecules must show their potential biological activity with good pharmacokinetic properties [40]. Pharmacokinetic profile of the compound has been evaluated through POM analysis [40,41]. POM can predict the type of pharmacophore site that influences the biological activity of a molecule [42]. In this study, several combined pharmacophore sites were identified in the compound by POM analysis. These were two antitumors

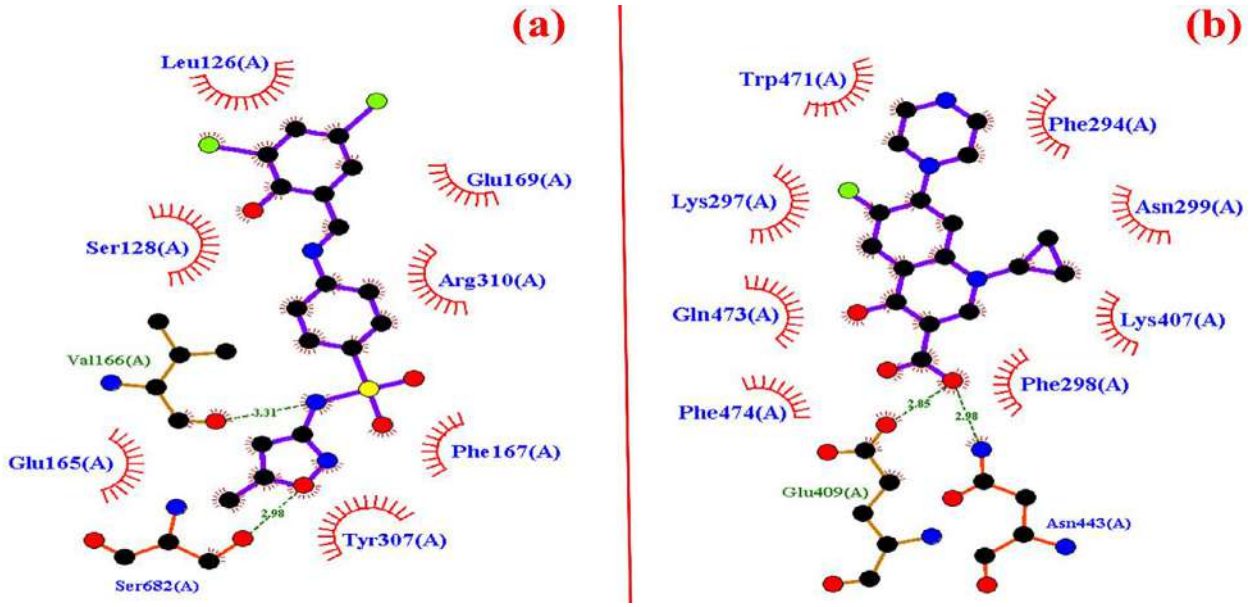

Fig. 12. Binding poses of the compound (a) and ciprofloxacin (b) with 4FQ4.

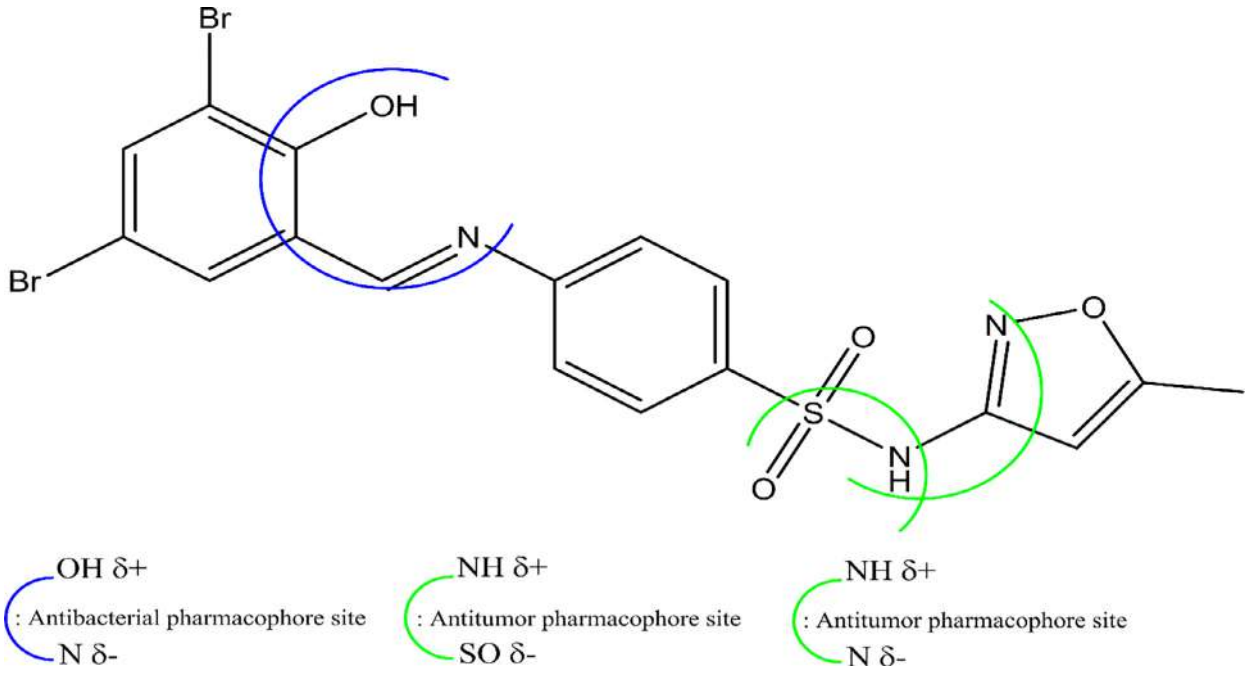

Fig. 13. Identification of antitumor and antibacterial pharmacophore sites.

($NH^{\delta+}$––$SO^{\delta-}$ and $NH^{\delta+}$––$N^{\delta-}$) and one antibacterial ($OH^{\delta+}$––$N^{\delta-}$) pharmacophore sites (Fig. 13).

In this study computer programmed OSIRIS explorer was used to predict the toxicity profiles as well as drug-likeness and overall drug score of the compound. The results suggested that it has no tumorigenic, mutagenic or irritant properties. It followed Lipinski's rule of five with one violation (mw 515.18) and exhibited promising drug-like character and drug score. Molecular properties and bioactivity score were assessed by Molinspiration. For better absorption and bioavailability, topological polar surface (TPSA) should be < 140 Å^2 with $\leq$10 rotatable bonds. The results of different molecular properties such as TPSA, hydrogen bond donors and acceptors, rotatable bonds were within the acceptable limit. The bioactivity score was calculated on the basis of kinase inhibitor, protease inhibitor, GPCR ligand, nuclear receptor ligand, ion channel modulator and enzyme inhibitor.

3.12. Antimicrobial and anti-inflammatory activity

Antimicrobial *i.e.*, antibacterial and antifungal properties were performed by disk diffusion method [43]. In this study, kanamycin and ketoconazole were used as standard. The compound was dissolved in DMSO, which was used as control. The results revealed that it exhibited potential antibacterial activity against *S. typhi* and *S. aureus*. For antifungal activity, the compound showed moderate inhibitory activity against both *A. niger* and *A. flavus*

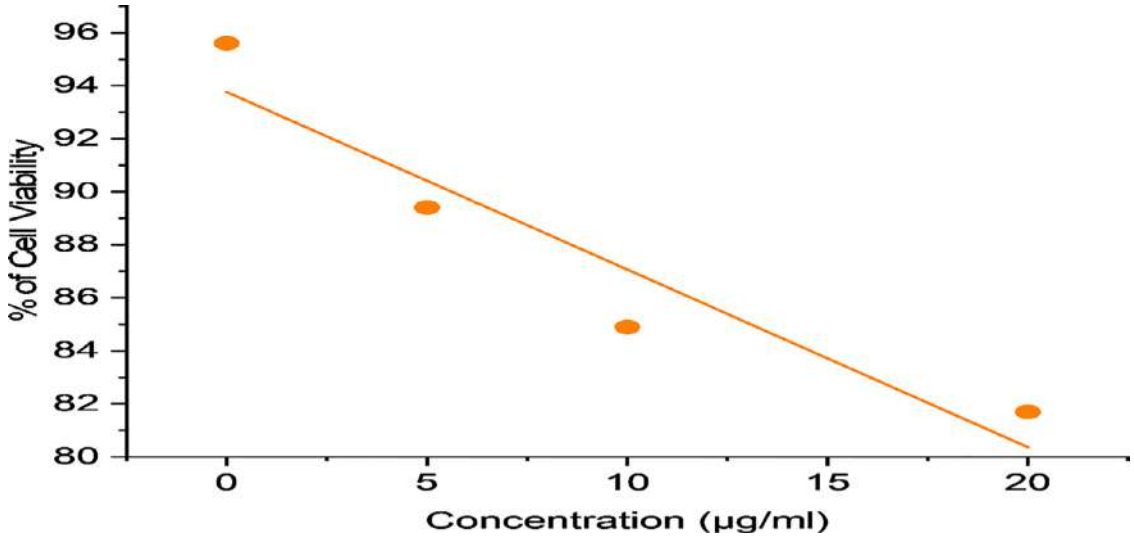

Fig. 14. The cytotoxic effect observed after incubation for 48 hrs.

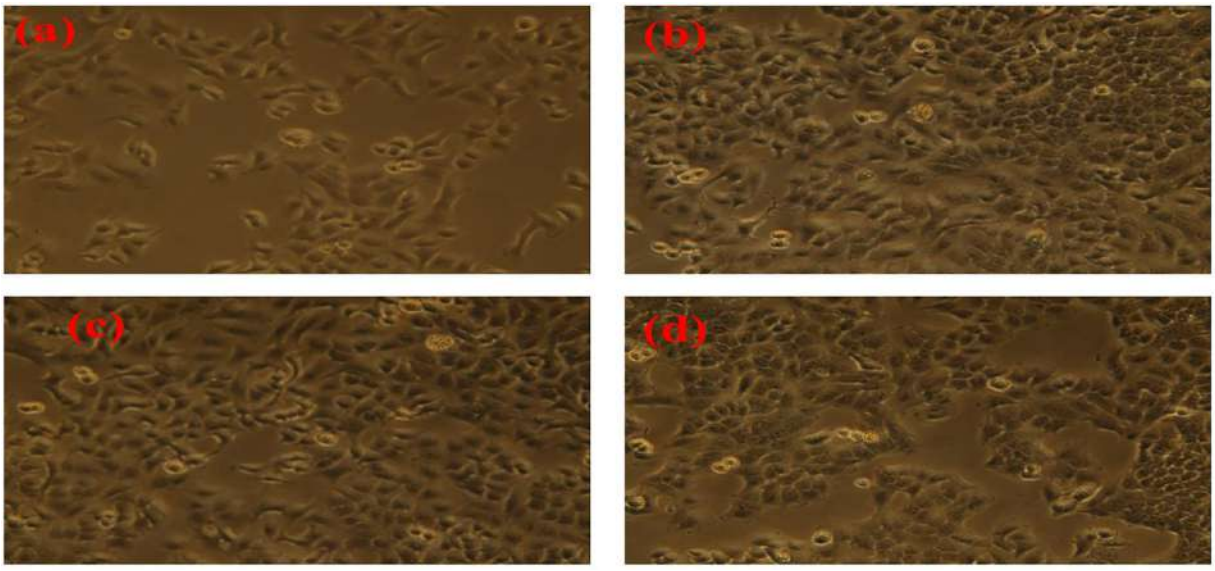

Fig. 15. Microscopic images of lung cancer A549 cells for control (a), 5 μg/mL (b), 10 μg/mL (c) and 20 μg/mL (d).

strains. Finally, the compound was also used to investigate the *in vitro* anti-inflammatory effect by human red blood cell (HRBC) membrane method [44]. The compound has the capability to stabilize the RBC membrane in hypotonic solution and protect hemolysis.

3.13. Cytotoxic activity

Cytotoxic activity of the compound was performed against lung cancer A549 cells. It exhibited cytotoxic activity with IC_{50} value of 65.34 μg/mL at 48 h cells incubation. Concentration *vs*% of cell viability curve (Fig. 14) represents a dose dependent effect of the compound. It was found that cell viability was reduced with the increased concentration of the compound. DMSO (1%) was used as negative control. Again, by using trypan blue staining, we found a clear difference between dead cells and live cells. Trypan blue binds with dead cells which was calculated by an automated cell counter (LUNA-II^{TM}, Analytikjena, South Korea). The compound induced cell death in A549 cells which was seen by inverted light microscopy (Fig. 15).

3.14. Free radical scavenging activity

The free radicals produced by oxidative reactions in the living body which are harmful. These radicals cause various diseases in the human body, such as cancer, diabetes, liver injury, cardiac diseases, and aging [45–47]. Butylated hydroxytoluene (BHT) is a popular antioxidant and used as standard. Because of its high reactivity with free radicals, it can protect the human body from damage caused by harmful radicals and play an important role in the curing and prevention of various diseases [46]. 2,2-diphenyl-1-picrylhydrazyl (DPPH) is a stable free radical substance which is widely used to evaluate the antioxidant activity of chemical species. Organic compounds having free phenolic hydroxyl groups are believed to have strong antioxidant activity {Formatting Citation}. The antioxidant activity of the compound was determined by DPPH radical scavenging assay with various concentrations (400, 200, 100, 50, 25, 12.5, 6.25 and 3.125 ppm) at 517 nm and the obtained result is shown in Fig. 16. The IC_{50} value of the compound was 4.25 μM and that of BHT was 2.56 μM. Therefore, the compound showed moderate antioxidant activity as compared to BHT.

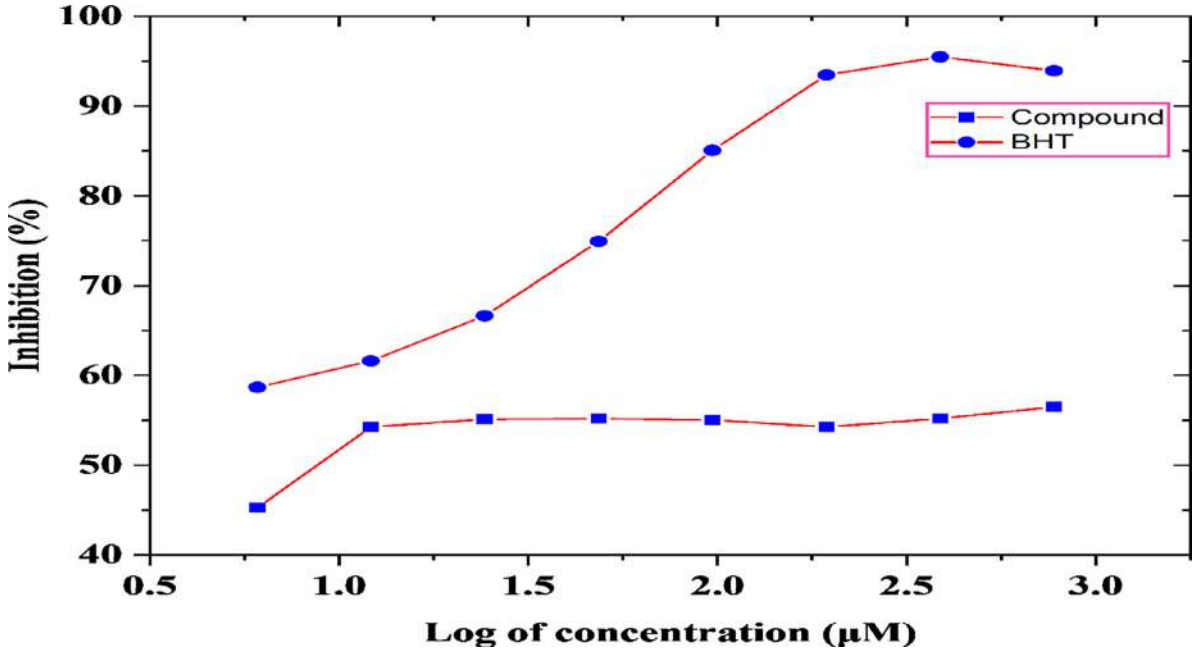

Fig. 16. Antioxidant activity of the compound.

4. Conclusion

In this study our newly synthesized compound was analyzed by various physico-chemical and quantum computational techniques. The compound has monoclinic structure with space group $P2_1/c$. Bond distance of C7=N1 was 1.277(5) Å. The structure was stabilized due to the presence of intramolecular hydrogen bond and weak $\pi-\pi$ stacking interactions. A FTIR band observed at 1616 cm^{-1} was characteristic to azomethine group. The proton of the azomethine group was given a signal at 8.94 ppm in NMR spectrum. The experimental findings of infrared, UV–vis, bond lengths, bond angles and torsion angles were in good agreement with computed data. The compound has high kinetic stability and good binding ability with biomolecules according to global reactivity descriptors results. Molecular docking study suggested that it showed higher binding energy as compared to ciprofloxacin. The antioxidant activity of the compound was found good and it showed promising antibacterial and antifungal effects. In addition, the studied compound exhibited remarkable anti-inflammatory activity and stabilizing capability of the RBC membrane in hypotonic solution. The cytotoxic activity of the compound was potent with IC_{50} value of 65.344 μg/mL.

Declaration of Competing Interest

The authors declare that there is no conflict of interests regarding the publication of this research paper.

CRediT authorship contribution statement

Subrata Paul: Conceptualization, Data curation, Formal analysis, Visualization, Writing – original draft, Writing – review & editing. **Md. Ashraful Alam:** Conceptualization, Investigation, Methodology, Supervision. **Tarun Kumar Pal:** Formal analysis, Investigation, Software, Supervision, Visualization, Writing – review & editing. **Md. Najem Uddin:** Data curation. **Md. Monirul Islam:** Software. **Md. Chanmiya Sheikh:** Methodology.

Acknowledgements

Tarun Kumar Pal is highly obliged to acknowledge the Director, Research & Extension, Rajshahi University of Engineering & Technology. Tarun Kumar Pal and Md. Chanmiya Sheikh are thankful to Ryuta Miyatake, University of Toyama, Japan for providing facilities for single-crystal X-ray analysis.

References

[1] F.D.S. Siqueira, G.G. Rossi, A.K. Machado, C.F.S. Alves, V.C. Flores, V.D. Somavilla, V.A. Agertt, J.D. Siqueira, R.D.S. Dias, P.M. Copetti, M.R. Sagrillo, D.F. Back, M.M.A. de Campos, Sulfamethoxazole derivatives complexed with metals: a new alternative against biofilms of rapidly growing mycobacteria, Biofouling 34 (2018) 893–911.
[2] N. Kausar, S. Muratza, M.A. Raza, H. Rafique, M.N. Arshad, A.A. Altaf, A.M. Asiri, S.S. Shafqat, S.R. Shafqat, Sulfonamide hybrid Schiff bases of anthranilic acid: synthesis, characterization and their biological potential, J. Mol. Struct. 1185 (2019) 8–20.
[3] W.A. Al-Masoudi, R.A. Faaz, R.H. Al-Asadi, H.S. Jabbar, Development and validation of a stability-indicating RP-LC method for the simultaneous determination of otilonium bromide and its expected degradation product in bulk drug and pharmaceutical preparation, Eur. J. Chem. 7 (2016) 102–106.
[4] M. Tahriri, M. Yousefi, K. Mehrani, M. Tabatabaee, M.D. Ashkezari, Synthesis, characterization and antimicrobial activity of two novel sulfonamide Schiff base compounds, Pharm. Chem. J. 51 (2017) 425–428.
[5] H.M.Z. El-Alfy, A.M. Hassan, E.S.A.E.H. Khattab, B.H. Heakal, Synthesis, characterization and biological evaluation studies of 4-((3-Formyl-4-hydroxyphenyl) diazinyl) -N-(4-methyloxazol-2-yl) benzene sulfonamide with Cu(II), Ni (II), Zn(II) and Ag(I) using a microwave irradiation, Egypt. J. Chem. 61 (2018) 569–580.
[6] E. Hejchman, H. Kruszewska, D. Maciejewska, B. Sowirka, M.Tomczyk Młynarczuk–Biały, A. Sztokfisz–Ignasiak, J. Jankowski, Design, synthesis and biological activity of Schiff bases bearing salicyl and 7–hydroxycoumarinyl moieties, Monatsh. Chem. 150 (2019) 255–266.
[7] A.S. Hassan, A.A. Askar, E.S. Nossier, A.M. Naglah, G.O. Moustafa, M.A. Al-Omar, Antibacterial evaluation, in silico characters and molecular docking of Schiff bases derived from 5-aminopyrazoles, Molecules 24 (2019) 1–12.
[8] A. Capan, S. Urus, M. Sonmez, Ru(III), Cr(III), Fe(III) complexes of Schiff base ligands bearing phenoxy groups : application as catalysts in the synthesis of vitamin K3, J. Saudi Chem. Soc 22 (2018) 757–766.
[9] M. Mesbah, T. Douadi, F. Sahli, S. Issaadi, S. Boukazoula, S. Chafaa, Synthesis, characterization, spectroscopic studies and antimicrobial activity of three new Schiff bases derived from Heterocyclic moiety, J. Mol. Struct. 1151 (2018) 41–48.

[10] A. Mumtaz, T. Mahmud, M. Elsegood, W. GW, Synthesis and characterization of new Schiff base transition metal complexes derived from drug together with biological potential study, J Nucl Med Radiat Ther 07 (2016) 1–4.

[11] D. Canakci, I. Koyuncu, N. Lolak, M. Durgun, S. Akocak, C.T. Supuran, Synthesis and cytotoxic activities of novel copper and silver complexes of 1,3-diaryltriazene-substituted sulfonamides, J. Enzyme Inhib. Med. 34 (2019) 110–116.

[12] M. Durgun, C. Türkeş, M. Işık, Y. Demir, A. Saklı, A. Kuru, A. Güzel, Ş. Beydemir, S. Akocak, S.M. Osman, Z. AlOthman, C.T. Supuran, Synthesis, characterisation, biological evaluation and in silico studies of sulphonamide Schiff bases, J. Enzyme Inhib. Med. 35 (2020) 950–962.

[13] R.D. Dennington, T.A. Keith, J.M. Millam, GaussView 6.0.16, Gaussian Inc, 340 (2008).

[14] M.J. Frisch, G.W. Trucks, H.B. Schlegel, G.E. Scuseria, M.A. Robb, J.R. Cheeseman, G. Scalmani, V. Barone, B. Mennucci, G.A. Petersson, H. Nakatsuji, M. Caricato, X. Li, H.P. Hratchian, A.F. Izmaylov, J. Bloino, G. Zheng, J.L. Sonnenberg, M. Hada, M. Ehara, K. Toyota, R. Fukuda, J. Hasegawa, M. Ishida, T. Nakajima, Y. Honda, O. Kitao, H. Nakai, T. Vreven, J.J.A. Montgomery, J.E. Peralta, F. Ogliaro, M. Bearpark, J.J. Heyd, E. Brothers, K.N. Kudin, V.N. Staroverov, R. Kobayashi, J. Normand, K. Raghavachari, A. Rendell, J.C. Burant, S.S. Iyengar, J. Tomasi, M. Cossi, N. Rega, J.M. Millam, M. Klene, J.E. Knox, J.B. Cross, V. Bakken, C. Adamo, J. Jaramillo, R. Gomperts, R.E. Stratmann, O. Yazyev, A.J. Austin, R. Cammi, C. Pomelli, J.W. Ochterski, R.L. Martin, K. Morokuma, V.G. Zakrzewski, G.A. Voth, P. Salvador, J.J. Dannenberg, S. Dapprich, A.D. Daniels, O. Farkas, J.B. Foresman, J.V. Ortiz, J. Cioslowski, D.J. Fox, Gaussian, Gaussian, Inc., CT Wallingford, 2009.

[15] C. Lee, W. Yang, R.G. Parr, Development of the Colie-Salvetti correlation-energy formula into a functional of the electron density, Phys. Rev. B. 37 (1988) 785–789.

[16] M. Katari, E. Nicol, V. Steinmetz, G. van der Rest, D. Carmichael, G. Frison, Improved infrared spectra prediction by DFT from a new experimental database, Chem. Eur. J. 23 (2017) 8414–8423.

[17] H. Abd El-Halim, M. Omar, M.N. Anwar, Preparation, characterization, antimicrobial and anticancer activities of Schiff base mixed ligand complexes, J. Therm. Anal. Calorim. 130 (2017) 1069–1083.

[18] N. Yildirim, N. Demir, G. Alpaslan, B. Boyacioğlu, M. Yildiz, H. Ünver, DFT calculation, biological activity, anion sensing studies and crystal structure of (E)-4-chloro-2-((pyridin-2-ylimino)-methyl)phenol, J. Serb. Chem. Soc. 83 (2018) 707–721.

[19] S. Alyar, T. Sen, Ü. €Ozdemir Ozmen, H. Alyar, S. Adem, Synthesis, spectroscopic characterizations, enzyme inhibition, molecular docking study and DFT calculations of new Schiff bases of sulfa drugs, J. Mol. Struct. 1185 (2019) 416–424.

[20] S. Mondal, S.M. Mandal, T.K. Mondal, C. Sinha, Structural characterization of new Schiff bases of sulfamethoxazole and sulfathiazole, their antibacterial activity and docking computation with DHPS protein structure, Spectrochim. Acta. A Mol. Biomol. Spectrosc. 150 (2015) 268–279.

[21] V. Pehlivan, E. Biçer, Y.G. Bekiroğlu, N. Dege, Electrochemical and spectroscopic studies on the interaction modes of calf thymus DNA with antibacterial Schiff bases obtained from substituted salicylaldehydes and sulfamethizole, Int. J. Electrochem. Sci. 13 (2018) 10700–10717.

[22] A.O. Yıldırım, M. Gulsu, C.A. Kastas, Synthesis, crystal structure and computational studies of a new Schiff base compound: imino] methyl}phenol, Acta Crystallogr. E. 74 (2018) 319–322.

[23] Y.H. Tan, S.G. Teoh, W.S. Loh, H.K. Fun, 4-[(2-H*ydroxy*-5-*nitrobenzylidene*)*amino*] benzenesulfonamide, Acta Crystallogr. E. 66 (2010) 2610–2611.

[24] Y.M. Chumakov, V.I. Tsapkov, G. Bocelli, B.Y. Antonsyak, S.A. Palomares-Sánches, R.S. Ortiz, A.P. Gulya, Crystal structures of condensation products of 3,5-dibromosalicylic aldehyde with streptocide, norsulfazole, and ethazole, J. Struct. Chem. 47 (2006) 933–939.

[25] Y.M. Chumakov, V.I. Tsapkov, G. Bocelli, B.Y. Antosyak, N-Acetyl-4-[(2-*hydroxybenzylidene*)-*amino*]benzenesulfonamide monohydrate and N-acetyl-4-[(5-*bromo*-2-*hydroxybenzylidene*)*amino*]benzenesulfonamide monohydrate, Acta Crystallogr. C. 61 (2005) 460–463.

[26] C. Dong, PowderX: windows-95-based program for powder X-ray diffraction data processing, J. Appl. Crystallogr. 32 (1999) 838.

[27] F.M. Anjalin, N. Kanagathara, M.K. Marchewka, V. Mohankumar, Crystal structure, Hirshfeld surface analysis and vibrational spectral studies on P-nitroanilinium p-toluene sulphonate single crystal, J. Mol. Struct. 1183 (2019) 78–86.

[28] M. Khalid, A. Ali, M.F.U. Rehman, M. Mustaqeem, S. Ali, M.U. Khan, S. Asim, N. Ahmad, M. Saleem, Exploration of noncovalent interactions, chemical reactivity, and nonlinear optical properties of piperidone derivatives: a concise theoretical approach, ACS Omega 5 (2020) 13236–13249.

[29] M. Khalid, A. Ali, M. Adeel, Z.U. Din, M.N. Tahir, E. Rodrigues-Filho, J. Iqbal, M.U. Khan, Facile preparation, characterization, SC-XRD and DFT/DTDFT study of diversely functionalized unsymmetrical bis-aryl-α, β-unsaturated ketone derivatives, J. Mol. Struct. 1206 (2020) 1–36.

[30] M.N. Arshad, M.M. Hussain, A.M. Asiri, M. Khalid, A.A.C. Braga, M.M. Rahman, A potent synthesis and supramolecular synthon hierarchy percipience of (E)-N′-(Napthalen-1-yl-methylene)-benzenesulfonohydrazide and 1-Napthaldehyde: a combined experimental and DFT studies, J. Mol. Struct. 1221 (2020) 1–25.

[31] R. Basri, M. Khalid, Z. Shafiq, M.S. Tahir, M.U. Khan, M.N. Tahir, M.M. Naseer, A.A.C. Braga, Exploration of chromone-based thiosemicarbazone derivatives: SC-XRD/DFT, spectral (IR, UV−Vis) characterization, and quantum chemical analysis, ACS Omega 5 (2020) 30176–30188.

[32] M. Khalid, M. Ali, M. Aslam, S.H. Sumrra, M.U. Khan, N. Raza, N. Kumar, M. Imran, Frontier molecular, natural bond orbital, uv-vis spectral study, solvent influence on geometric parameters, vibrational frequencies and solvation energies of 8-hydroxyquinoline, Int. J. Pharm. Sci. 8 (2017) 457–469.

[33] M. Asad, M.N. Arshad, S.A. Khan, M. Oves, M. Khalid, A.M. Asiri, A.A.C. Braga, Cyclization of chalcones into N-propionyl pyrazolines for their single crystal X-ray, computational and antibacterial studies, J. Mol. Struct. 1201 (2020) 1–35.

[34] R.S. Correa, K.M. Oliveira, H. Perez, A.M. Plutin, R. Ramos, R. Mocelo, E.E. castellano, A.A. Batista, H. Pe, Cis-bis (N-benzoyl-N′, N′-dibenzylthioureido) platinum (II): synthesis, molecular structure and its interaction with human and bovine serum albumin, Arab. J. Chem 12 (2019) 3454–3462.

[35] A. Ali, M. Khalid, Z.U. Din, H.M. Asif, M. Imran, M.N. Tahir, M. Ashfaq, E. Rodrigues-Filho, Exploration of structural, electronic and third order nonlinear optical properties of crystalline chalcone systems: monoarylidene and unsymmetrical diarylidene cycloalkanones, J. Mol. Struct. 1241 (2021) 1–11.

[36] M. Ashfaq, A. Ali, A. Kuznetsov, M.N. Tahir, M. Khalid, DFT and single-crystal investigation of the pyrimethamine-based novel co-crystal salt: 2,4-diamino-5-(4-chlorophenyl)-6-ethylpyrimidin-1-ium-4-methylbenzoate hydrate (1:1:1) (DEMH), J. Mol. Struct. 1228 (2021) 1–27.

[37] S.K. Wolff, D.J. Grimwood, J.J. McKinnon, M.J. Turner, D. Jayatilaka, M.A. Spackman, Wolff, S.K., D.J. Grimwood, J.J. McKinnon, M.J. Turner, D. Jayatilaka, and M.A. Spackman, Crystal Explorer. (2012).

[38] T.K. Pal, M.A. Mumit, J. Hossen, S. Paul, M.A. Alam, M.A.A.A.A. Islam, M.C. Sheikh, Computational and experimental insight into antituberculosis agent, (E)-benzyl-2-(4-hydroxy-2-methoxybenzylidene) hydrazinecarbodithioate: ADME analysis, Heliyon. 7 (2021) 1–6.

[39] M. Mumit, T. Kumar, A. Alam, A. Islam, S. Paul, C. Sheikh, DFT studies on vibrational and electronic spectra, HOMO-LUMO, MEP, HOMA, NBO and molecular docking analysis of benzyl-3-N-(2,4,5- trimethoxyphenylmethylene) hydrazinecarbodithioate, J. Mol. Struct 1220 (2020) 1–11.

[40] M.I.S. Abdelhady, A.M. Kamal, M.F. Barghash, POM analyses, immunomodulatory, cytotoxic activities and polyphenolic constituents of Callistemon viridiflorus fruits, Bull. Fac. Pharm. 56 (2018) 175–178.

[41] S. Bawazer, A. Khan, A. Rauf, T.B.E.N. Hadda, Y.S. Al-Awthan, O. Bahattab, U. Rashid, I. Khan, M.A. Nawaz, M.S. Uddin, O. Ahmed, M.A. Shariati, POM analysis and computational interactions of 8-hydroxydiospyrin inside active site of protein tyrosine phosphatase 1B, Biocell 45 (2021) 751–759.

[42] K. Bechlem, M. Aissaoui, B. Belhani, K.O. Rachedi, S. Bouacida, R. Bahadi, S.E. Djouad, R. Ben Mansour, M. Bouaziz, F. Almalki, T. Ben Hadda, M. Berredjem, Synthesis, X-ray crystallographic study and molecular docking of new α-sulfamidophosphonates: POM analyses of their cytotoxic activity, J. Mol. Struct. 1210 (2020) 1–23.

[43] M.Y. Nassar, H.M. Aly, E.A. Abdelrahman, M.E. Moustafa, Synthesis, characterization, and biological activity of some novel Schiff bases and their Co(II) and Ni(II) complexes: a new route for Co3O4 and NiO nanoparticles for photocatalytic degradation of methylene blue dye, J. Mol. Struct. 1143 (2017) 462–471.

[44] G. Banuppriya, R. Sribalan, V. Padmini, Synthesis and characterization of curcumin-sulfonamide hybrids: biological evaluation and molecular docking studies, J. Mol. Struct. 1155 (2018) 90–100.

[45] W. Li, X. Qiao, Z. Wang, S. Wang, S. Chen, Synthesis and antioxidant activity of conjugates of hydroxytyrosol and coumarin, Bioorg. Chem. 105 (2020) 1–48.

[46] T. Afsar, S. Razak, M. Shabbir, M.R. Khan, Antioxidant activity of polyphenolic compounds isolated from ethyl – acetate fraction of Acacia hydaspica R . Parker, Chem. Cent. J. 12 (2018) 1–13.

[47] H. Li, D. Zhang, L. Tan, B. Yu, S. Zhao, W. Cao, Comparison of the antioxidant properties of various solvent extracts from Dipsacus asperoides and identification of phenolic compounds by LC-ESI-QTOF-MS–MS, S. Afr. J. Bot. 109 (2017) 1–8.